Supplement of Clim. Past, 19, 2287–2311, 2023
https://doi.org/10.5194/cp-19-2287-2023-supplement

Climate of the Past
Open Access
EGU

Supplement of

Southern Hemisphere atmospheric history of carbon monoxide over the late Holocene reconstructed from multiple Antarctic ice archives

Xavier Faïn et al.

Correspondence to: Xavier Faïn (xavier.fain@univ-grenoble-alpes.fr)

Summary

S1. Methodology

S1.1. Location of drilling and firn air sampling sites

Figure S1. Location of the different ice core drillings (DC12, Berkner Island (BKN), and TaldIce (TD)) and firn air sampling (DE08-2, DSSW19K and DSSW20K on Law Dome; Lock In (LI), South Pole (SP), and ABN) sites. The CSIRO stations conducting atmospheric monitoring and discussed in this study are also reported (Mawson, Casey, and South Pole).

S1.2. Ice core chronologies

All gas age scales reported in this study (i.e., DC12, ABN, TD, and EDML-B40) are tied to the WDC06A-7 chronology.

Ice core	Δage (yrs)	Reference
DC12	2400	Fourteau et al., 2020
ABN	630	Servettaz et al., 2023
TaldIce	615	*This study*
EDML- B40	811	Rhodes et al., 2016

Table S1. Gas chronology for ice cores featured in this study. Δage reports the difference between gas age and ice age. All gas age scales are tied to the WDC06A-7 chronology.

S1.3. Calibration of CO datasets

NOAA and CSIRO have maintained CO measurement programs and separate calibration scales over more than three decades. NOAA is the WMO-designated Central Calibration Laboratory for CO with their data currently reported on the WMO-X2014 scale. Long-term intercomparison programs involving NOAA and CSIRO revealed large concentration-dependent differences in the 1990s (Masarie et al., 2001). Thus CSIRO elected to maintain its own calibration scale. The current version of the CSIRO scale (CSIRO2020) is closely aligned with WMO-X2014 in terms of absolute concentration but its internal consistency and long-term stability are constrained by internal CSIRO procedures and remain entirely independent of WMO-X2014 assignments. Ongoing refinement of calibration scales at both laboratories has led to much improved agreement between the respective scales, with differences now within ±1 ppb over the range of 28 - 487 ppb (Langenfelds et al., 2023).

CO measurements (including firn and ice cores) are conducted with a SARA optical analyzer (OF-CEAS, Morville et al., 2005) at IGE. CSIRO uses gas chromatography for determination of [CO] in firn air samples (Langenfelds et al., 2023). Such methodologies differ from NOAA, which applies a VURF detection (https://www.esrl.noaa.gov/gmd/ccl/co_scale.html) for CO mixing ratios. All firn air CO datasets included in this study except Berkner Island (BKN) and Lock-In (LI) datasets were analyzed at CSIRO and are reported on the CSIRO2020 scale. Ice core datasets (analyzed at IGE and DRI) and the LI firn air dataset (analyzed at IGE) are reported on the WMO-X2014 scale. [CO] drifts within cylinders were quantified, either at CSIRO or at IGE. Specifically, the standard gases used for calibrating dataset at IGE were first certified at NOAA in 2012, and recertified in 2020 by the EU ICOS network (https://www.icos-cp.eu/). Very limited drifts in [CO] were observed, ranging 0.1 - 0.2 ppb per year depending on cylinders. The standard gas cylinders used to calibrate the ABN ice core dataset were certified at NOAA just prior to the CFA campaign.

In this study, we combine CO data produced in different laboratories, principally CSIRO (Australia) and IGE (France). The good agreement between CSIRO2020 and WMO-X2014 (Langenfelds et al., 2023) allows for the combination of datasets reported on either scale to produce a coherent paleo-atmospheric CO history.

For each analytical campaign at IGE (including CFA campaigns and Lock-In firn air sample measurements), the OF-CEAS spectrometer was carefully calibrated on dry gas by direct injection of a synthetic standard gas (Scott Marin, artificial gas mixtures). Finally, during each analytical campaign (CFA and firn air measurements), routine measurements of a gas standard verified that no drift was occurring, and that the calibration of the OF-CEAS analyzer was remaining stable.

S1.4. Internal precision of CO CFA analyzes

Allan-Werle variance tests (Allan, 1966, Werle et al., 1993) applied to calibration loop dataset (deionized degassed water mixed with a single standard gas) in order to evaluate Internal precision and stability of gas-CFA measurements are reported on Fig. S2. Internal precision, defined as twice the Allan-Werle deviation at chosen integration time, was 0.7 and 1.0 ppb for the IGE (i.e., DC12 and TD) and DRI (i.e., ABN) analytical campaigns (Table S2).

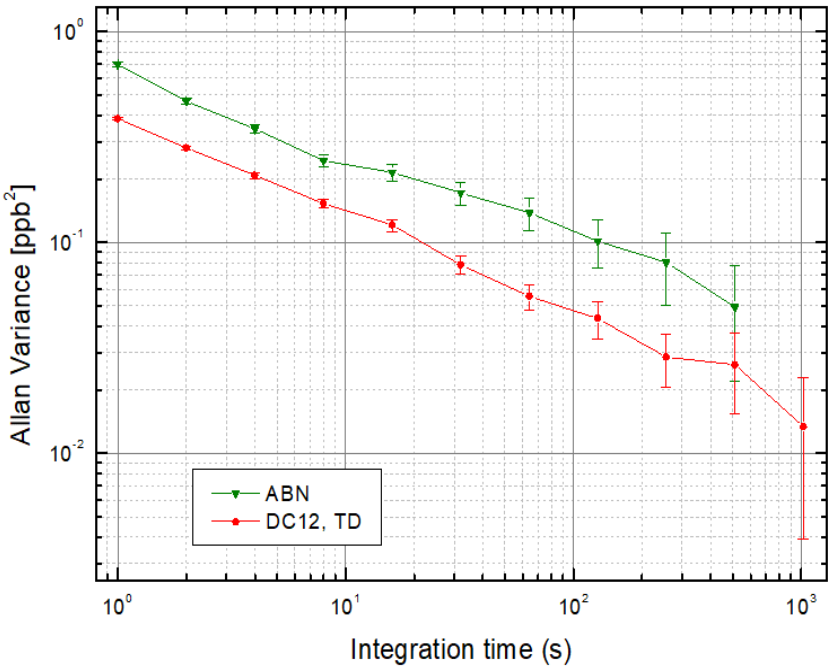

Figure S2. Allan-Werle variance results for calibration loop dataset (DI degassed water mixed with a single standard gas) collected for the different CFA setups: DRI (ABN core) and IGE (DC12 and TD cores).

Ice core	Laboratory of analysis	Analysis date	Mean gas sample flow (sccm min^{-1})	Optimal Integration Time (s)	Integration Time applied (s)	Internal precision at IT (ppb) (2σ)	External precision (ppb) (2σ)	System response time (min)	CO blank (ppb)	CO solubility losses (%)
EDML-B40	DRI	10-14/10/2013	1.50	n.d.	10	n.d.	n.d.	14.2	n.d.	6.0%
DC12	IGE	6-24/06/2014	1.35	>1000	10	0.7	2.8	1.6	4.1	7.4%
TD	IGE	17-21/10/2014	1.45	>1000	10	0.7	2.8	1.6	4.1	7.4%
ABN	DRI	5-14/10/2015	1.62	>500	10	1.0	8.8	9.3	7.4	6.0%
Solarice	IGE	15/01/2019	1.30	>1000	10	0.7	8.8	1.6	4.1	7.4%

Table S2. CFA setup specifications and performances of the different analytical campaigns.

S1.5. External precision of CO CFA analyzes

External precision of the continuous CO measurements (i.e., including all sources of errors or bias) can be investigated by melting replicate ice sticks on different days on a gas-CFA setup. Such an approach has been applied before to CFA gas setups (Faïn et al., 2022). Specifically, we define the external precision as the pooled standard deviations calculated on the differences of CO concentrations from main (M) and replicate (R) analyzed ice sticks, averaging continuous CO data over n intervals few cm long, following the formula

$$\sqrt{\frac{1}{2n}\sum([CO]_M - [CO]_R)^2}.$$

No long sections (i.e., > 1 meters) of replicate ice sticks were available or analyzed in the frame of this study to evaluate external precision directly on Antarctica ice samples. External precision for the IGE and DRI continuous CO measurements are thus extracted from the comparison of main and replicate analyzes conducted on the PLACE core, although this archive exhibits higher [CO] compared to Antarctic ice. The PLACE core was drilled in 2015 nearby Summit Station, Central Greenland, and analyzed in 2015 and 2017 at DRI and IGE, respectively (Faïn et al., 2022).

[CO] patterns extracted from the PLACE core exhibit high frequency variability, with high amplitude spike (i.e., amplitude larger than 100 ppb is observed, Faïn et al., 2022). Such patterns are different from continuous [CO] extracted from Antarctica ice, which reveals no in-situ production and no high-frequency, non-atmospheric, features (Fig. 2). Specifically, the difference between the maxima and minima of [CO] observed in our Antarctic high resolution CFA records is ~15 ppb (Fig. 2). Therefore, only sections of the PLACE record exhibiting minimum [CO] but within a range of 15 ppb were considered for the evaluation of external precisions for Antarctica samples.

In practice, 14.2 m (resp., 1.9 m) of replicate PLACE sticks analyzed at DRI in 2015 (resp., at IGE in 2017) were first considered. CO concentrations measured on both main and replicate ice sticks were averaged by binning over 142 10-cm long (resp., over 190 1-cm long) intervals at DRI (resp., at IGE). Second, 33 (resp., 33) intervals were selected at DRI (resp., IGE) for exhibiting minimum [CO] of the Greenland records, and within a range of 15 ppb. Figure S3 reports significant correlations between averaged [CO] from main cuts versus averaged [CO] from replicate cuts for both CFA setups. Finally, 2σ external precision of 2.8 ppb (resp. 8.8 ppb) was calculated for the IGE CFA setup (resp., the DRI CFA setup).

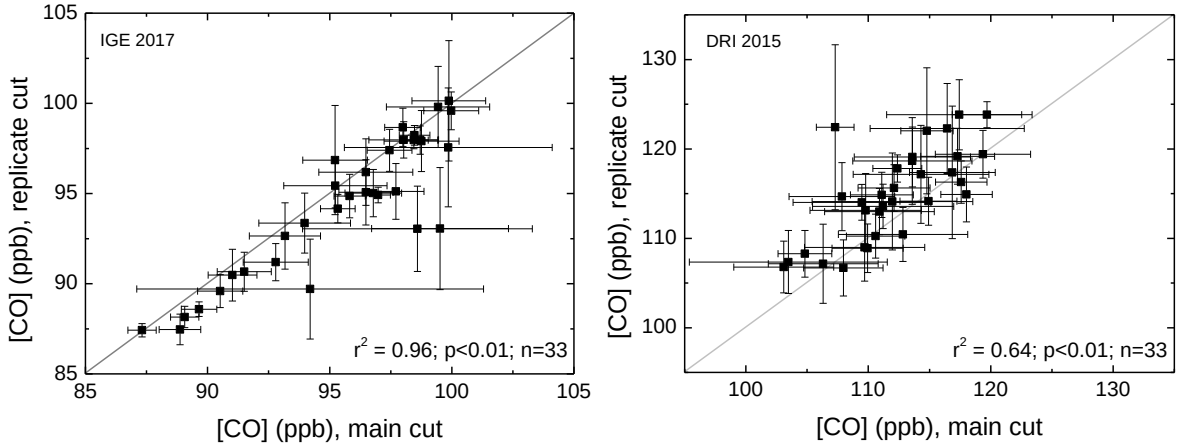

Figure S3. CO mixing ratios measured on both main and replicate PLACE ice sticks at IGE (left panel) and DRI (right panel), after averaging data over 1-cm long (resp., over 10-cm long) intervals at IGE (resp., at DRI). The 1:1 line is shown in grey.

S1.6. Absolute calibration of continuous CO datasets: accuracy

A fraction, or all, of gases dissolved in the water CFA sample flow are not recovered by the Idex degassers used in this study. CO solubility is higher than N_2 or O_2 solubility. This preferential dissolution of CO in comparison to N_2 and O_2 results in underestimated CO mixing ratios when detected at the gas outlet of the degasser. This underestimation of CO mixing ratios need to be accurately quantified so as to provide an absolute calibration of CO continuous dataset.

In this study, we follow the rationale reported by Faïn et al. (2022) and use the calibration loop (CL) to calibrate internally (i.e., with CFA data) continuous CO datasets. We hypothesise that CO and methane dissolution follow the same physical laws: consequently, if a calibration loop is able to reproduce methane preferential dissolution, it should also reproduce CO losses related to dissolution. Estimates of methane losses related to dissolution, independent of the calibration loop, from each ice core analyzed, was thus required. For the ice core DC12, preferential methane dissolution was already known (Fourteau et al., 2020). For the ABN and TD archives, it was evaluated by direct comparison of CFA dataset with WAIS-Divide discrete record (Mitchell et al., 2013). Finally, we observed an underestimation of methane mixing ratios of 11.1%, 9.5%, and 11.1% when measuring the DC12, ABN, and TD cores, respectively.

Each continuous CO dataset, after initial calibration of the OF-CEAS analyzer (Sect. 1.2), was calibrated according to the following: $[CO]_{COR} = ([CO]_{SAMPLE} - CO_{BLANK}) / SC$

With SC the Solubility Correction evaluated with the CL experiment, and CO_{BLANK}, the CO blank of the CFA setup.

SC was extracted from multi-standard (with [CO] ranging 30-100 ppb) CL experiments. We operated the CL with different artificial gas cylinders of known CO and CH_4 mixing ratios. Liquid and gas flows injected through the CL were chosen to reproduce ice air content value. Gas flow was later adjusted if required so as the calibration loop reproduces nicely the expected methane preferential dissolution. At IGE, we were also able to add to the CL experiment an injection of CO-depleted air (so called “Air Zero” later), produced by flushing room air on a PtO trap heated at 200°C. After and/or before each calibration loop experiment, gas from all cylinders and Air Zero were analyzed directly with the OF-CEAS analyzer. The CL data were not calibrated onto the WMO-X2014 scale, but instead directly compared to these direct measurements from cylinders or Air Zero. The same calibration was applied to both datasets collected with the IGE setup, i.e. DC12 and TD (Fig. S4). Indeed (i) similar CH_4 preferential dissolutions were observed during the DC12 and TD analyzes, and (ii) configuration of IGE CFA setup remains identical for the DC12 and TD analytical campaigns. Similarly, the calibration applied to the ABN dataset is identical to the one previously used by Faïn et al., (2022) to calibrate the PLACE dataset. The ABN core was analyzed immediately after the PLACE core, with no changes within the CFA setup, and similar CH_4 preferential dissolution was observed during the PLACE and ABN analyzes. The CO blanks of the IGE and DRI setups have been reported previously (Faïn et al., 2022) and are reported in Table S2, along with SC.

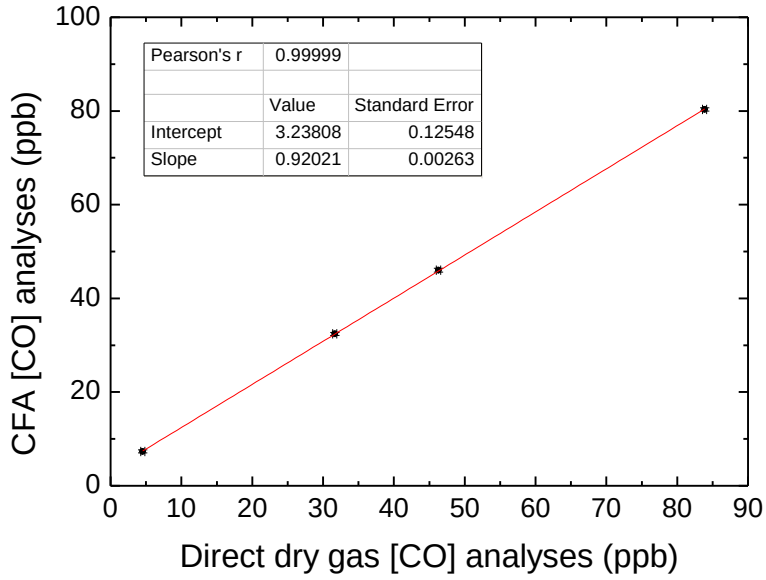

Figure S4. Multi-standard Calibration Loop experiment conducted on the IGE CFA setup: CO preferential dissolution representative of the DC12 and TD melting conditions. The intercept indicates the CO blank level during the experiment, and is in agreement with the CO system blank established previously for the IGE CFA setup (i.e., 4.1±1.2 ppb, Table S2; Faïn et al., 2022).

S2. Supporting Data

S2.1. CSIRO atmospheric [CO] monitoring in Antarctica

CSIRO has measured CO in flask samples of background air from a range of SH sites since the 1980s. Antarctic sites with long CO records include Mawson (MAA, since 1984), South Pole (SPO, since 1991) and Casey (CYA, since 1996). Samples were pressurized in CSIRO's 0.5L or 5.0L glass flasks using customised pump units equipped with either chemical (anhydrous magnesium perchlorate) or cryogenic drying (Francey et al., 2003; Langenfelds et al., 2023). The MAA dataset is used as the primary link to firn/ice data in this study due to its longer duration and MAA's coastal Antarctic location being similar to that of Law Dome.

Gas chromatographic (GC) measurements since 1991 were made using a Trace Analytical Reduction Gas Analyzer (RGA). These records are supported by extensive measurements of a large suite of calibration standards, including ten CO-in-synthetic-air standards in the range of approximately 23 - 200 ppb that were prepared by Scott Marrin, USA in 1992 and which retain about 1/3 of their original contents. Random uncertainties applying to these flask sample CO data are generally within ±1 ppb. Systematic uncertainties relevant to comparison with firn/ice data are dominated by two components:

(i) Correction for flask storage effects. Measured CO in CSIRO's 0.5L glass flasks with PFA o-rings is corrected by -0.0058 ppb/day of storage (equivalent to -2.1 ppb yr^{-1}), as derived from multiple, mainly laboratory-based storage tests. However, drift rates can vary depending on flask history, condition and CO content of the atmosphere in which the flasks are stored. Because MAA samples are returned to CSIRO in annual batches, mean corrections are approximately -1.4 ppb with an estimated uncertainty of ±1 ppb in MAA annual means.

(ii) Long-term calibration drift. Uncertainty in stability of the CSIRO2020 scale over three decades is estimated at ±0.1 ppb yr^{-1}, based on the measured relative stability of a large number of air samples/standards stored in a range of different cylinder types, and supporting results from other experimental tests of instrument and air standard stability (Masarie et al., 2001).

GC measurements of earlier MAA samples (1984 - 1990) were made with one of two Carle instruments where CO was catalytically converted to CH_4 for flame ionisation detection (FID). Data from this period are not supported by similar levels of calibration and other diagnostic data as applied to the RGA data (Langenfelds et al., 2023). These early data are noisier and carry larger uncertainty in scale stability of ±0.57% yr^{-1} (equivalent to approx. ±0.24 ppb yr^{-1} in

CO mole fraction observed at that time; Langenfelds et al., 2023). Consequently, they are not used in this study.

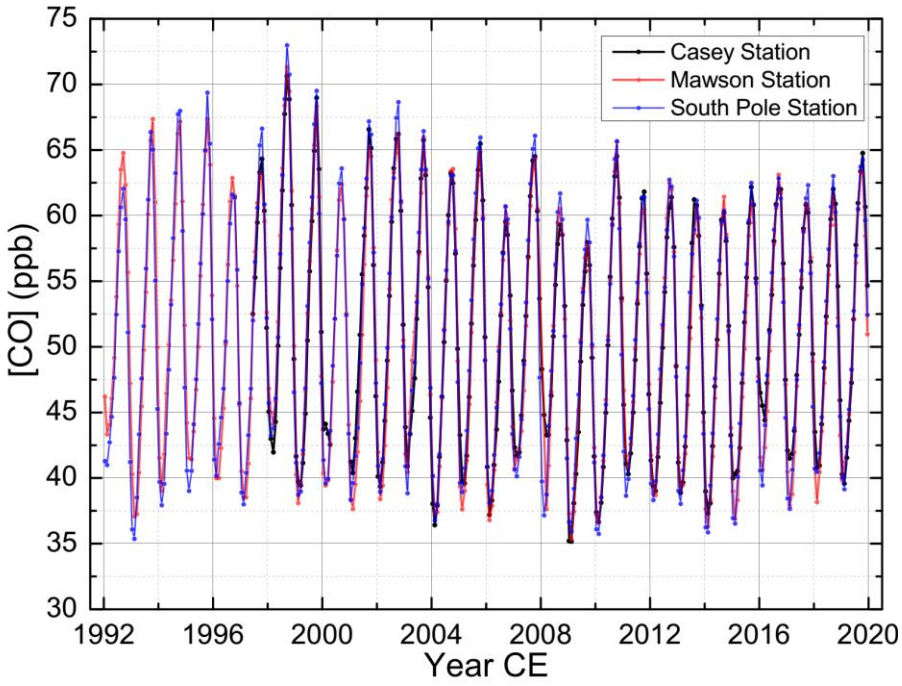

Figure S5. Monthly mean records from flask measurements of [CO] by CSIRO at Casey (Loh et al., 2021a), South Pole (Loh et al., 2021b), and Mawson (Loh et al., 2021c) stations (Antarctica), for the time period spanning 1992-2020 CE. Data are reported on the CSIRO2020 CO scale.

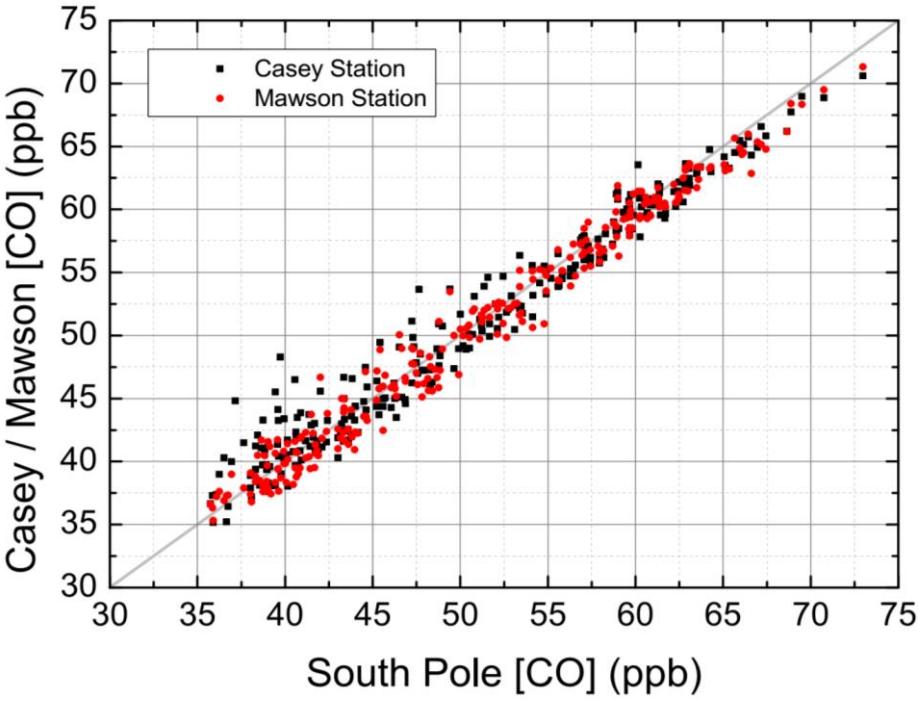

Figure S6. Correlation (r^2 = 0.96) of the CSIRO monthly mean records from flask measurements of [CO] from Casey (Loh et al., 2021a), South Pole (Loh et al., 2021b), and Mawson (Loh et al., 2021c) stations, for the period spanning 1997-2020 CE. Data are reported on the CSIRO2020 CO scale. The grey line indicates the 1:1 line.

S2.2 Firn air measurement uncertainty

The precision of the firn air [CO] measurements can be estimated from replicate measurements of samples collected at the same level for each site. The 2-sigma precision is about 1 ppb for all sites, except for DE08-2 where it is about 2 ppb. The accuracy, including possible effects of the firn air sampling device (FASD) tubing, bladder and pumps, sample storage in the flask and subsequent measurement, is more difficult to estimate. Comparisons of "surface" firn air [CO], where the FASD inlet is at the snow surface, with "reference" atmospheric [CO] concentrations from air sampled into flasks directly at the site, or with the CO measurements at the coastal stations, mainly Mawson (both firn measurements and station measurements being on the same scale) may reveal sampling artifacts. This assumes that the "reference" measurements are accurate and are representative of the air being sampled at the firn air sampling location and time by the FASD. The comparison is also limited by the sample size- typically only a few surface firn air sample measurements are made. Also, the deepest levels, where the firn air sample flow can be very low and pumped at well below ambient pressures, can be challenging to sample reliably, and may not be closely simulated by the FASD at the surface (sampling at ABN simulated sub ambient pressure in the inlet line by placing a restriction on the FASD inlet, with no detectable systematic effect on [CO]). The comparison of surface firn [CO] with reference atmospheric [CO] gives differences of about ±1 ppb.

S2.3. IGE-GIPSA firn inversion

S2.3.1. Depth-concentration firn [CO] profiles

As mentioned in the caption of Fig. 1 in the main manuscript, comparing the [CO] firn data plotted as a function of mean age with the modeled atmospheric trend is not entirely rigorous due to the distributed gas ages resulting from diffusive mixing in the firn. Here we more appropriately compare the [CO] observed and modeled in the firn air. To model [CO] we used the atmospheric trend obtained by inverse firn modeling as input to the forward firn model. The best guess results and uncertainty envelopes illustrate the ability of the model to simultaneously represent the five datasets (Fig. S7).

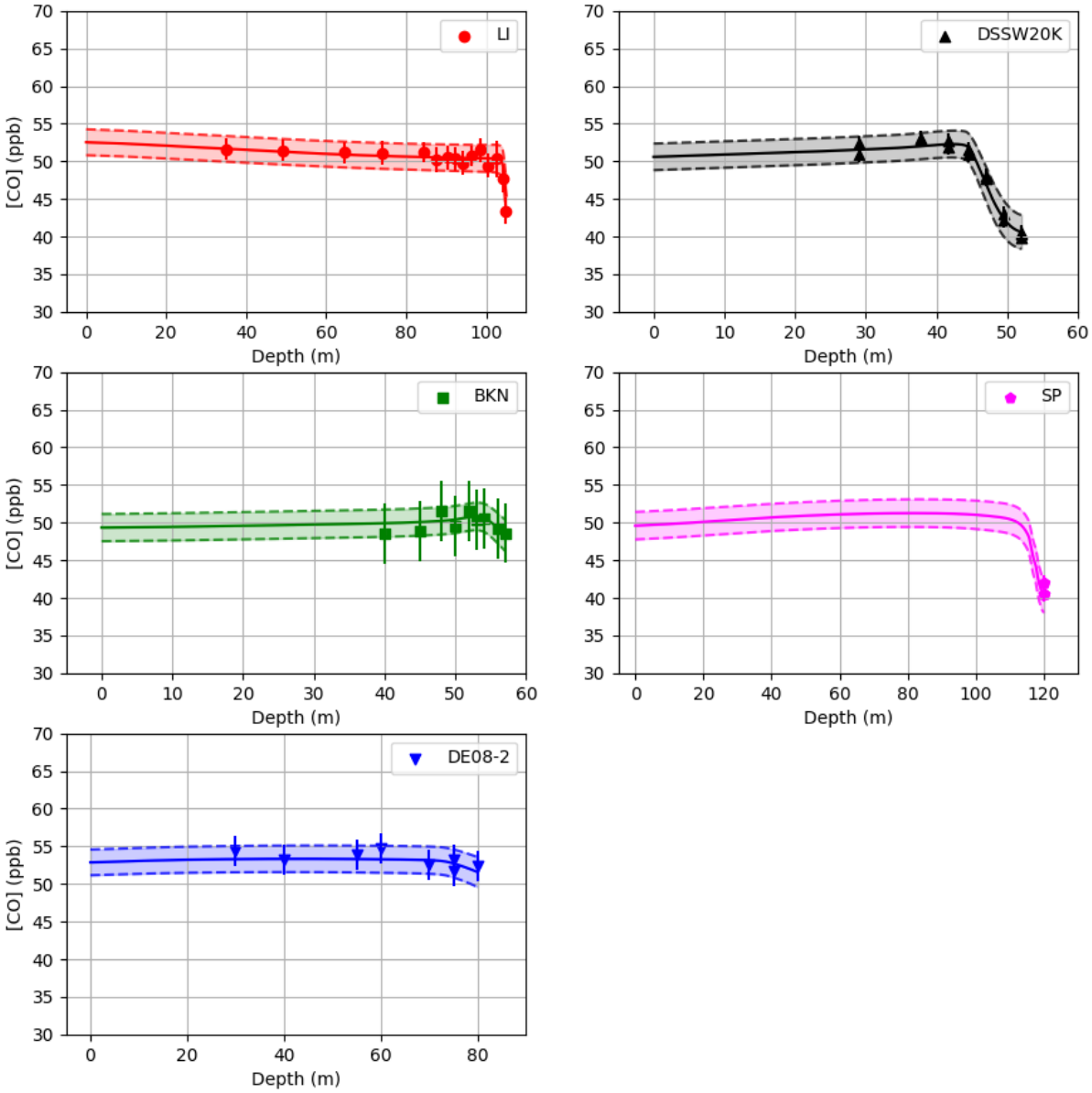

Figure S7. Concentration-depth profiles in the firn air at the five sites investigated with the IGE-GIPSA model. The measurements are reported with symbols with error bars indicating 2σ uncertainties (when available). The solid lines are best fits of the firn IGE-GIPSA model, with envelopes indicating the 2σ uncertainties.

S2.3.2. Constraints from ice core dataset

As introduced in Sect. 2.4 of the main manuscript, simulations were performed with the IGE-GIPSA model with and without constraints from ice core data in addition to firn air data. The two tests are compared in Fig. S8. The multi-site record based on a spline-fit to the ice core data presented in Section 3.3.2 is used to build five synthetic data points in BKN ice at 70, 71, 72, 73 and 74 meters depth. BKN is used as a substitute for the ABN site, which has almost the same accumulation rate. The Green's function approach was used to calculate mean gas

ages at the selected depth levels in BKN ice, then CO mixing ratios at the same gas-age in the multi-site spline-fit, ranging between 1862 and 1889 CE, were used to build the five synthetic data points shown on the lower left side of Fig. S8. The time trend scenarios obtained with (in black) and without (in grey) constraints in ice remain within the uncertainty envelopes of one another on their common time frame. Using the ice constraint allows us to reconstruct a trend that goes further back in time.

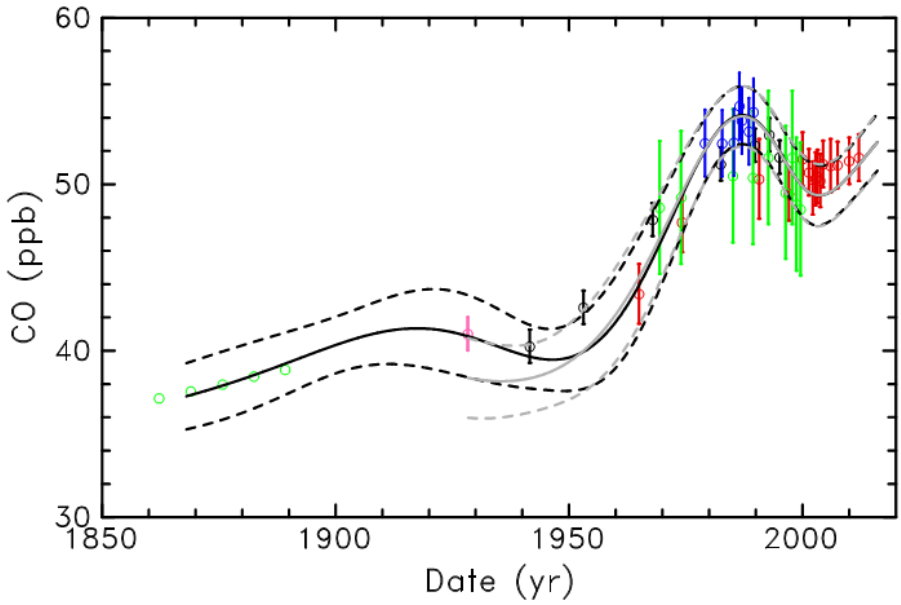

Figure S8. Modeled time trends of CO mixing ratios (continuous lines) with uncertainty envelopes (2σ, dashed lines) obtained with (in black) and without (in grey) synthetic ice core constraint. Synthetic ice core data are shown as green open circles on the left side of the plot (before 1900 CE) whereas firn air data are shown as open circles with uncertainties plotted as vertical bars, LI in red, DSSW20K in black, BKN in green, SP in pink, and DE08-2 in blue. We should note that firn air data plotted versus mean age are not strictly comparable to the modeled time trends which are determined using the age distributions for the samples from the firn model. This effect is most important near maxima or minima of the trend that are smoothed in the data.

S2.4. CSIRO firn inversion

The results from the CSIRO inverse model described in the main paper are obtained by using the CO ice reconstruction up to 1897 and the Mawson atmospheric record from 1993, and inferring the atmospheric history between 1898 and 1992 from the firn measurements. Here we give more details about that calculation, and show results from alternative calculations that do not use the ice reconstruction or the Mawson record. The CSIRO inverse model is implemented in IDL (Exelis Visual Information Solutions, Boulder, Colorado) using the

constrained_min routine. Non-negativity constraints such as those used by Trudinger et al. (2016) for PFCs are not useful in our inversion for CO because the mole fraction is far from zero and can decrease in time. A simple prior estimate of the CO atmospheric history is used as a starting point for the inversion, but is not included in the cost function. The results were found not to be sensitive to the prior estimate (after 1898, see next paragraph).

We include the ice reconstruction (black line in Fig. 3) in the inversion by setting the prior estimate to match the ice reconstruction up to 1897 and not allowing the inversion to update these values. The Green's functions for the deep firn that extend before 1898 are therefore convolved with a history that is part ice reconstruction and part firn reconstruction. We include the Mawson atmospheric history by using the firn model to calculate the influence at the measurement depths of the Mawson record interpolated to daily resolution from mid-1992 and mean seasonality before 1992, then subtracting this from the firn measurements prior to the inversion. We include the Mawson record in this way because the Mawson record needs to be modeled at about daily resolution to give accurate variation of CO with depth in the upper firn, and the Green's functions (saved at annual resolution) could not do this. Figure S9 shows the contribution of the different parts of the atmospheric history (i.e., up to 1897, between 1898 and 1992 and after 1993) to the modeled firn depth profiles.

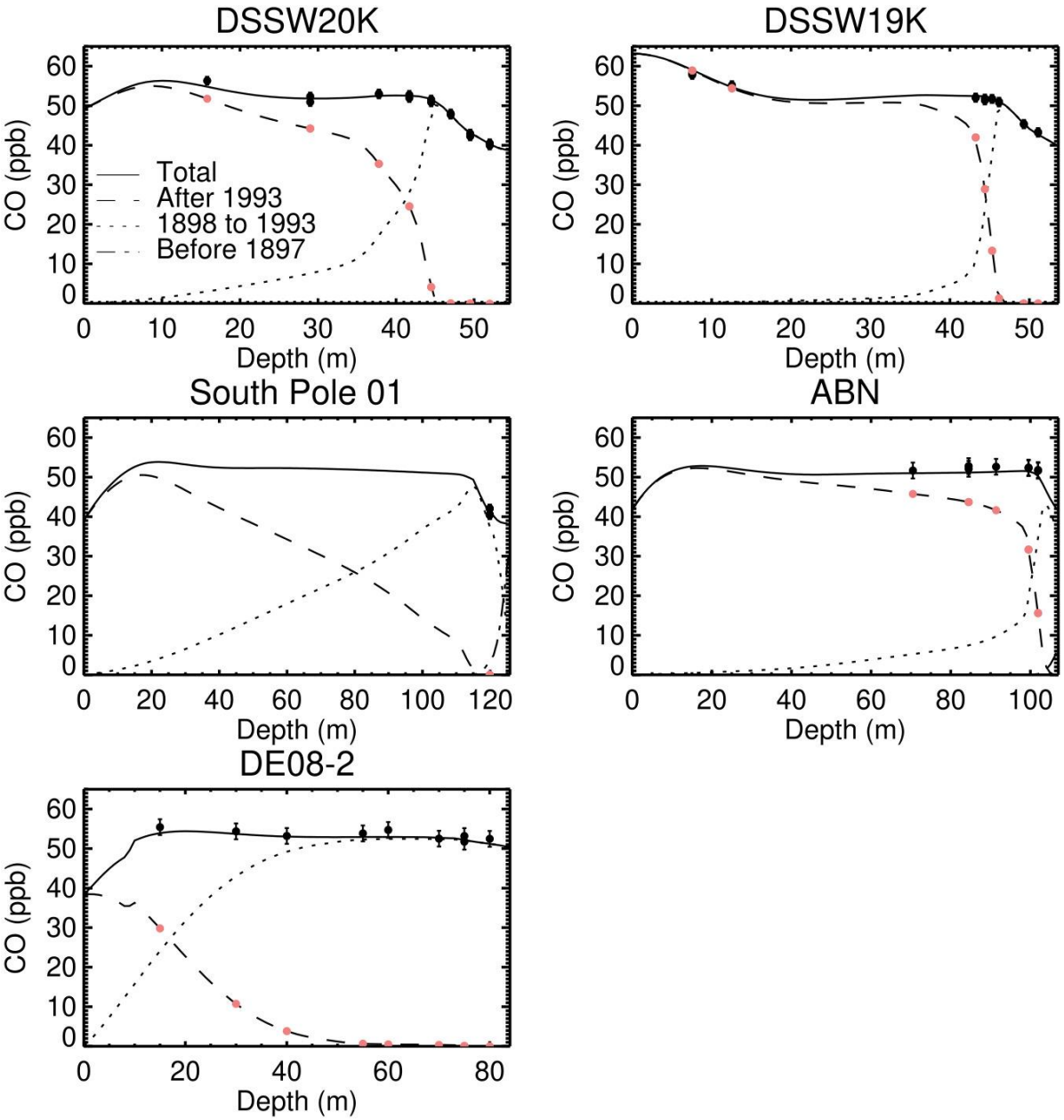

Figure S9. Modeled depth profiles of [CO] inversions from the CSIRO firn model at five sites (DSSW20K, DSSW19K, South Pole 01 (SP), ABN and DE08-2) showing the contribution of the atmospheric history up to 1897 (from the ice reconstruction), between 1898 and 1992 (inferred from the firn measurements) and after 1993 (from the Mawson atmospheric record). The black symbols show the actual firn measurements, and the pink symbols show the modeled influence of the Mawson record at the measurements depths.

The CSIRO inverse model uses bootstrapping to estimate uncertainties in the atmospheric CO reconstruction due to uncertainties in the firn measurements, the firn model, the ice reconstruction and the Mawson record. That is, we repeat the inversion more than 1000 times with the firn observations perturbed according to their uncertainty, using different firn model

Green's functions from an ensemble generated during firn model calibration (Trudinger et al., 2013), and ice reconstruction and Mawson record realizations that have been perturbed according to their respective uncertainties. The ice reconstruction is taken to have random uncertainties of 3.7 ppb before 1880 and 8.8 ppb after 1880 (see Sections 2.6.2 and S1.5, these are 2σ estimates of external precision from replicate ice sticks, modeled in the CSIRO inversion as random perturbations to annual values of the ice reconstruction) and systematic uncertainties due to the blank (2.8 ppb) and solubility (0.4 ppb), both 2σ, each modeled as a separate perturbation that is constant for each realization of the ice reconstruction in the inversion). In general, realizations of the ice reconstruction that are higher (on average) lead to firn reconstruction solutions that are lower, and vice versa, so that the convolution with the Green's function provides a similar match to the firn observations. The Mawson record uncertainties are dominated by systematic uncertainty due to the correction for flask storage effects (the same uncertainty for all years) and long-term calibration drift (higher uncertainty in early years, decreasing linearly with time) - see Sect. 2.1 and Langenfelds et al., (2023). These uncertainties are modeled in the CSIRO inversion by including random perturbations in the influence of the Mawson records at the firn measurement depths that are subtracted from the firn measurements before the inverse calculation. The maximum size of the perturbations has been determined with the firn model based on worst-case scenarios (specified at daily resolution) for errors in the Mawson record; the flask storage effect varies seasonally but averages about 1.4 ppb over a year, and the calibration drift is 3 ppb in 1992 decreasing linearly to zero now (these are taken to be 3σ).

We also consider a case without the ice reconstruction. In this case, the inversion infers the CO history back to 1900 and assumes constant CO levels up to 1900. No information about the ice reconstruction is used in this case. The inferred history differs by up to about 1 ppb from the case that uses the ice reconstruction, well within the uncertainty range. In addition, we consider a case without the Mawson record, and instead infer the atmospheric history up to 2004 from firn measurements below 25m (to avoid the influence of the seasonal cycle). These results are shown in Fig. S10, with all solutions showing good consistency.

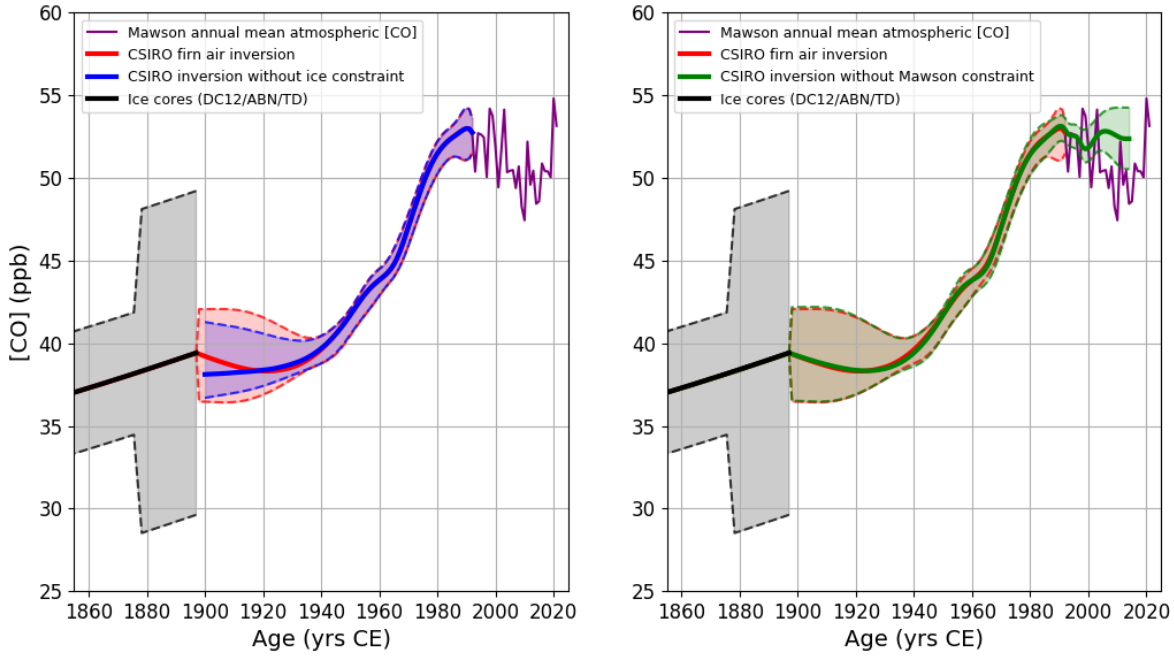

Figure S10. [CO] atmospheric reconstruction from the CSIRO inverse model with ice constraint (red line), and without ice constraint (blue line). The difference between the two inversions in 1897 CE is 1 ppb. The grey envelope shows the ice core record.

345

S2.4.1. Depth-concentration firn [CO] profiles

Figure S11 shows modeled concentration-depth profiles of CO in firn air from the CSIRO model. The solid lines correspond to the best fit cases in Fig 1f. The 2-sigma uncertainty band is generated by calculating firn depth profiles from the multiple atmospheric histories that result
350 from the bootstrap method, thus corresponding to the uncertainty range in Fig 1f.

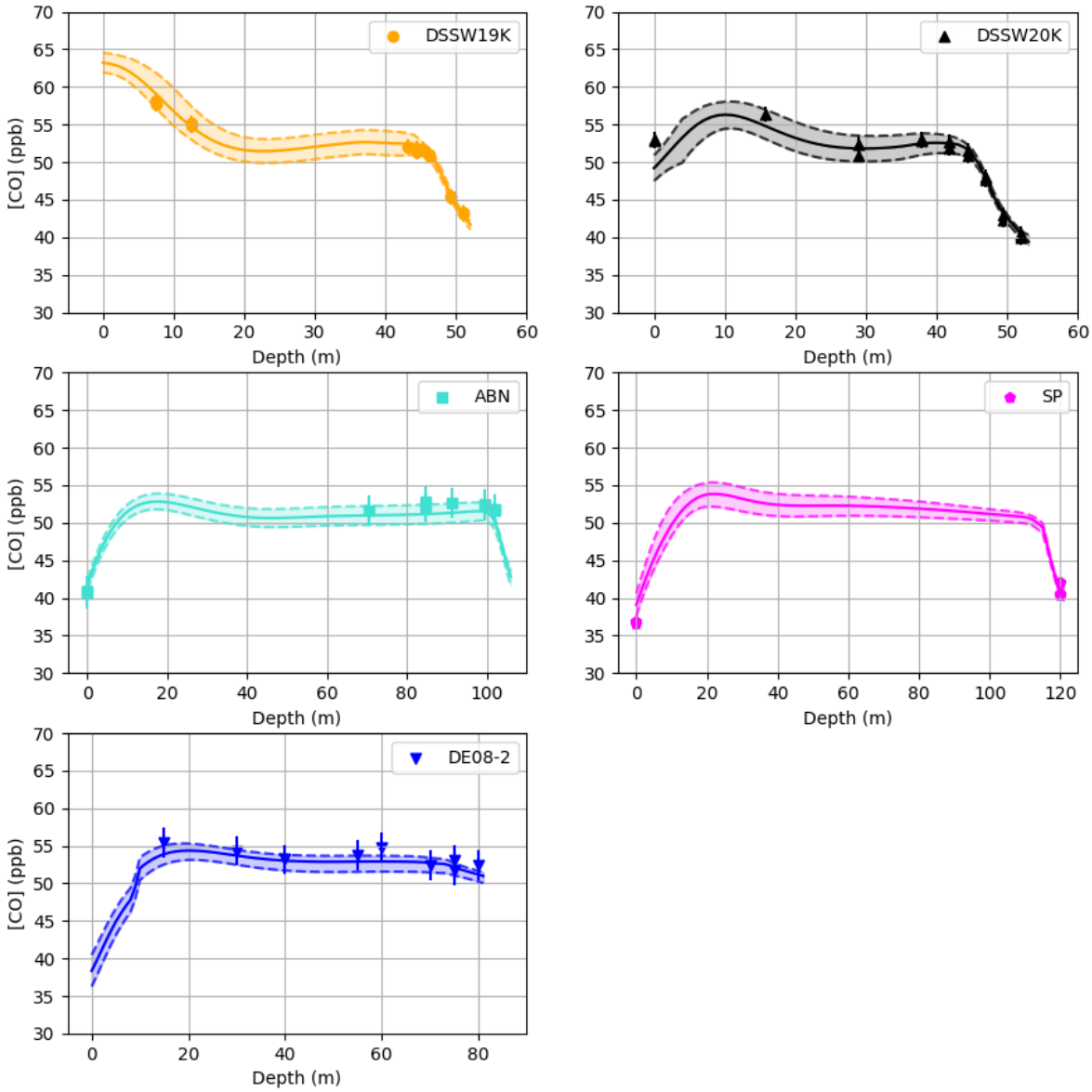

Figure S11. Concentration-depth profiles in the firn air at the five sites investigated with the CSIRO model. The measurements are reported with symbols with error bars indicating 2σ uncertainties. The solid lines are best fits of the firn CSIRO model, with envelopes indicating the 2σ uncertainties.

S2.5. Combining IGE-GIPSA and CSIRO firn reconstructions

In this study, we use two independent models as a way to incorporate firn model uncertainty. Over the period spanning 1905 to 1992, we average the IGE-GIPSA and CSIRO records' annual values to produce a multimodel firn air CO reconstruction. For the 1897-1904 CE period, a third order polynomial weight was introduced in the annual averaging of the two firn records. Such approach (Fig. S12) allowed (i) to weight the multimodel record toward the CSIRO reconstruction in 1897 CE (because it is continuous with the ice reconstruction), and

(ii) to match the [CO] growth rates (ie. in ppb yr^{-1}) of the firn and ice core reconstructions in 1897 and 1905 CE. The multimodel firn air reconstruction is reported in Fig. S12, along with IGE-GIPSA and CSIRO reconstructions. The envelopes represent 2σ uncertainty intervals.

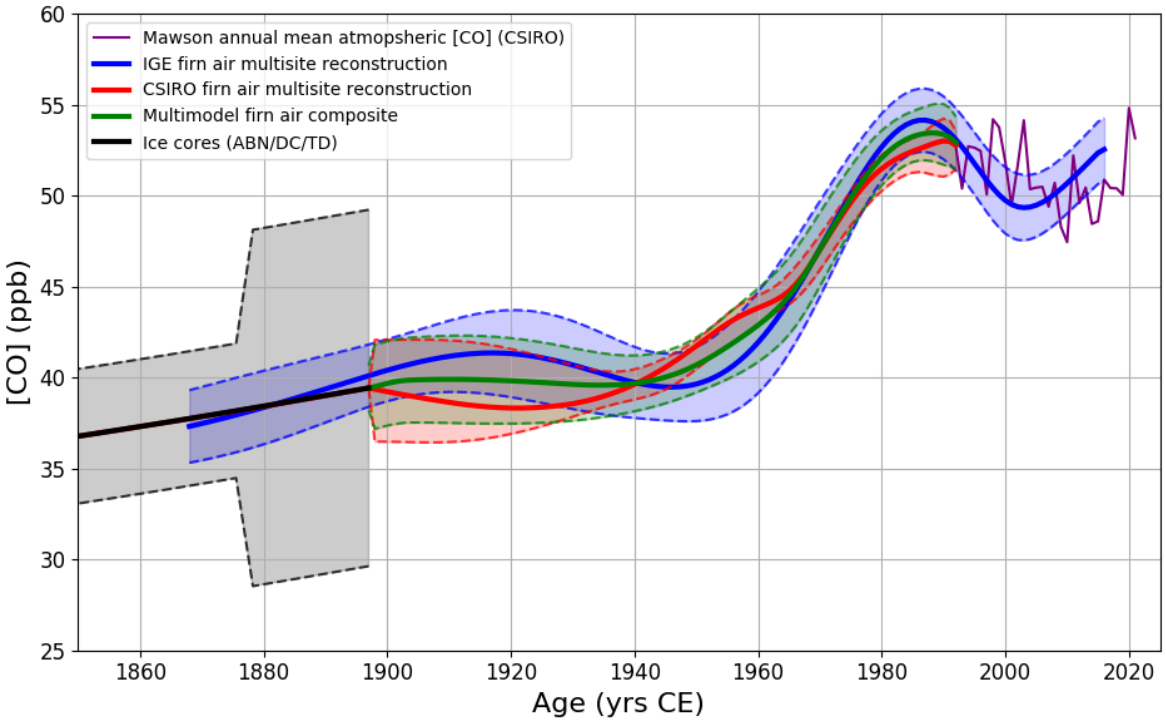

Figure S12. Optimal atmospheric [CO] history obtained with IGE-GIPSA (blue line) and CSIRO (red line) models. The green line shows the multimodel record obtained by averaging the IGE-GIPSA and CSIRO records.

S2.6. The EDML-B40 continuous CO dataset

The EDML-B40 (later referenced as B40 in this section) ice core was drilled close to Kohnen Station, Dronning Maud Land, East Antarctica, by the Alfred Wegener Institute (drilling site : 75.001◦ S, 0.068◦ E, 2911 m elevation, Fig. S1 and Table S3). This core was analyzed on the DRI CFA setup in September 2013 with a focus on methane mixing ratio (Rhodes et al., 2016). However, we were able to simultaneously measure CO concentrations, making the B40 core the first Antarctic ice archive measured for CO by CFA. As a first attempt to analyze continuously low-levels [CO] preserved in Antarctica ice, the B40 dataset is affected by memory effects and unexplained contaminations when initializing melting. Consequently, these data are not robust, and could not be calibrated and reported as absolute values. The configuration of the B40 analyzes is reported in Table S2.

Ice core & location (Fig. S1)	Depth intervals (m)	Gas age interval (yrs CE)	Accum. Rate (cm weq yr^{-1})	Mean annual Temp. (°C)
EDML - B40	97.0 - 99.0	1849 ;1878	6.3 [a]	-46 [a]
Dronning Maud Land	100.3 - 103.9	1781 ; 1833		
75°S, 0° E	107.2 - 109.9	1698 ; 1736		
2911 m elevation	115.2 - 116.3	1606 ;1623		
	117.6 - 119.7	1560 ; 1590		
Solar-Ice	150.0 - 158.7	-71 ; 27	2.5 [b]	-53 [c]
Dôme Concordia				
75°0.6' S, 133°2' E				
3233 m elevation				

385 **Table S3.** Locations, site characteristics and other relevant information for the EDML-B40 and Solar-Ice ice cores. [a]Klein et al. (2014), [b]Gautier et al. (2016), [c]Fabre et al. (2000).

Figure S13 reports raw CO data from the B40 core, and highlights in black decreasing CO trends systematically observed when initializing melting.

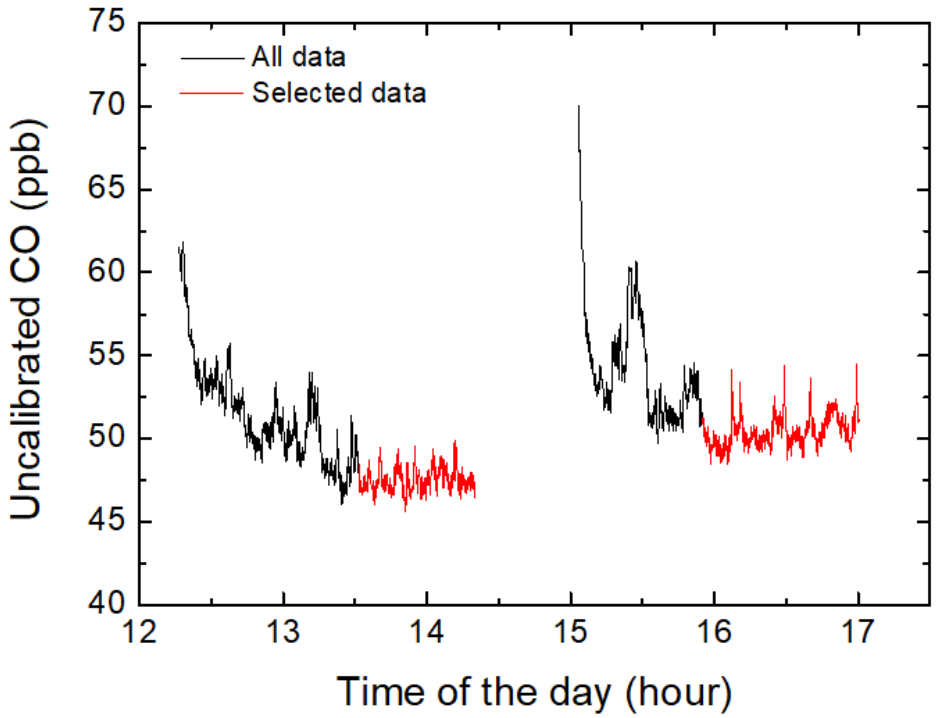

390 **Figure S13.** Typical EDML-B40 raw continuous CO data collected at DRI in September, 2013. Each analytical run lasts ~2 hours, and no sample is melted between runs. Decreasing trends in CO mixing ratio were observed at the beginning of each run, lasting for about half of the run.

In this Supplement, we extract the fraction of the B40 that we consider not affected by these contamination, i.e., for each melting run lasting about 2 hours, we kept the last hour of measurement (reported in red on Fig. S13). This is a conservative approach, but we preferred not applying CFA calibration to these data as the contamination processes were unexplained.

Finally, the selected, uncalibrated, B40 CO data are compared with other continuous Antarctica [CO] reconstruction (Fig. S14). To ease this comparison, we further apply an arbitrary offset of -19 ppb to the B40 data. B40 data show a trend similar to the DC12, ABN, and TD records. Specifically, the adjusted B40 data reproduce the minimum in [CO] observed at the beginning of the XVIII century, and the 10 ppb increases during the period extending to the onset of the Industrial Era. Although not accurate, the B40 data strengthen the pattern extracted from the calibrated record of the DC12, ABN and TD ice cores.

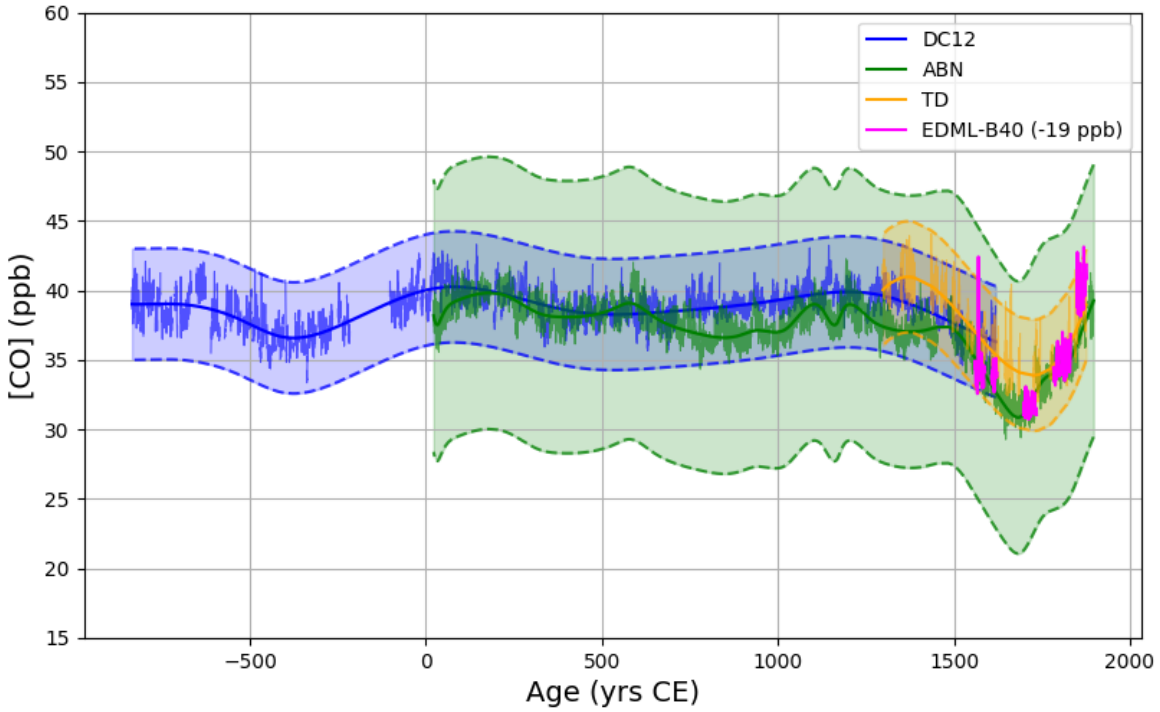

Figure S14. A selection of EDML-B40 [CO] data compared to continuous CO records of DC12, ABN and TD. The EDML-B40 data could not be CFA-calibrated, and were adjusted with an arbitrary offset of -19 ppb for the purpose of this comparison.

S2.7. Filling a gap in the DC12 dataset with the Solarice archive

The DC12 ice core was of extremely good quality, with very few breaks. However, a single section, spanning [154-158] m depth, was damaged during transportation and could not be

analyzed. To fill this gap, we took advantage of the Solarice core, drilled in 2016 at Concordia Station (75°0.6' S, 123°2' E) closely to the DC12 drilling site

A Solarice core section spanning [151.0 – 158.8] m depth was analyzed in January 2019 with the IGE CFA setup. Fig. S15 reports DC12 and Solarice datasets, with both cores calibrated with the same SC and Blank value (Table S2). The IGE CFA setup indeed remains unchanged between the two analytical campaigns, and the two ice cores originate from the same location.

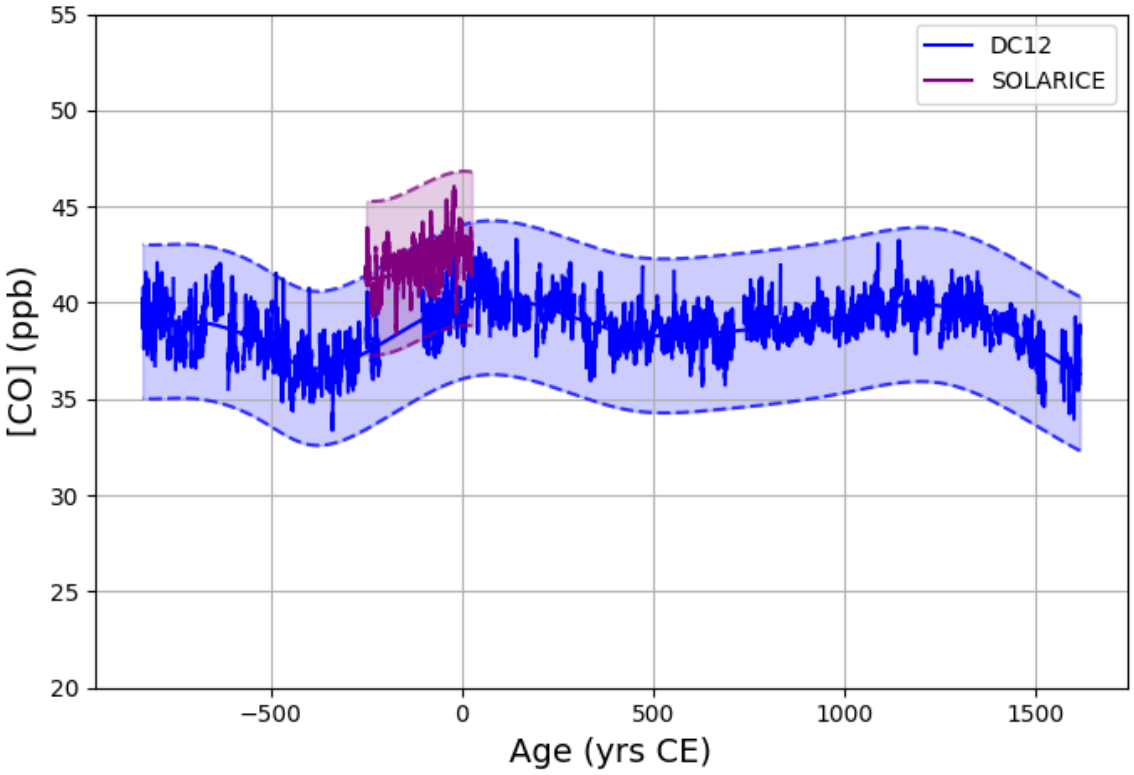

Figure S15. Solarice [CO] measurements conducted on the 150-158 m depth interval, overlapping with the gap in the DC12 record. Both Solarice and DC12 cores were drilled at Concordia Station (in 2016 and 2012, resp.), with boreholes located 2 km apart.

Although we observed slightly higher CO mixing ratios for Solarice compared to DC12, both records agree within their uncertainty envelope (2σ). The Solarice dataset reveals that [CO] remains very stable over the [151.0 – 158.8] depth range for ice drilled at the Dome Concordia, Antarctica. Consequently, we used a continuous spline to extract an average CO history from the high resolution DC12 signals.

S2.8. Localisation of charcoal records

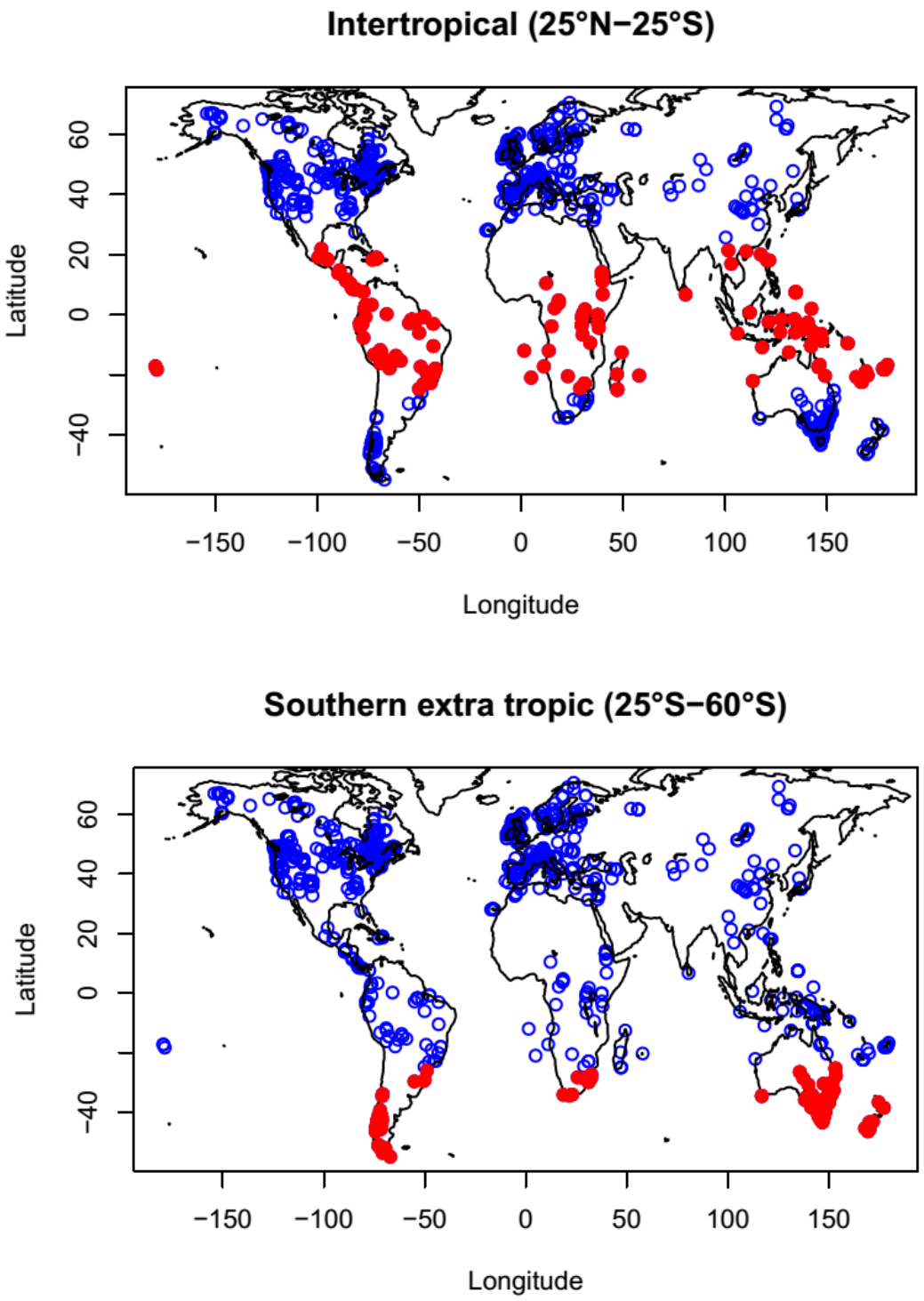

435 **Figure S16.** Localisation of charcoal records included in the composites discussed in this study (Fig. 5). Extracted from the Global Paleofire Database (https://database.paleofire.org).

S3. References

Allan, D. W.: Statistics of atomic frequency standards, Proc. IEEE, 54(2), 221–230, doi:10.1109/PROC.1966.4634, 1966.

Fabre, A., Barnola, J. M., Arnaud, L. and Chappellaz, J.: Determination of gas diffusivity in polar firn: comparison between experimental measurements and inverse modeling, Geophys. Res. Lett., 27(4), 557–560, 2000.

Faïn, X., Rhodes, R. H., Place, P., Petrenko, V. V., Fourteau, K., Chellman, N., Crosier, E., McConnell, J. R., Brook, E. J., Blunier, T., Legrand, M. and Chappellaz, J.: Northern Hemisphere atmospheric history of carbon monoxide since preindustrial times reconstructed from multiple Greenland ice cores, Clim. Past, 18(3), 631–647, doi:10.5194/cp-18-631-2022, 2022.

Fourteau, K., Martinerie, P., Faïn, X., Ekaykin, A. A., Chappellaz, J. and Lipenkov, V.: Estimation of gas record alteration in very low-accumulation ice cores, Clim. Past, 16(2), 503–522, doi:10.5194/cp-16-503-2020, 2020.

Francey, R. J., L. P. Steele, D. A. Spencer, R. L. Langenfelds, R. M. Law, P. B. Krummel, P. J. Fraser, D. M. Etheridge, N. Derek, S. A. Coram, L. N. Cooper, C. E. Allison, L. Porter and S. Baly, The CSIRO (Australia) measurement of greenhouse gases in the global atmosphere, *Baseline Atmospheric Program (Australia) 1999-2000,* N. W. Tindale, N. Derek and P. J. Fraser (eds.), Bureau of Meteorology and CSIRO Atmospheric Research, Melbourne, Australia, 42-53, 2003.

Fraser, P., S. Coram and N. Derek (1994), Atmospheric methane, carbon monoxide and carbon dioxide by gas chromatography, Baseline Atmospheric Program (Australia), A. L. Dick and J. L. Gras (eds.), Bureau of Meteorology and CSIRO Division of Atmospheric Research, Melbourne, Australia, 60-64, 1991.

Gautier, E., Savarino, J., Erbland, J., Lanciki, A. and Possenti, P.: Variability of sulfate signal in ice core records based on five replicate cores, Clim. Past, 12(1), 103–113, doi:10.5194/cp-12-103-2016, 2016.

Klein, K.: Variability in dry Antarctic firn – Investigations on spatially distributed snow and firn samples from Dronning Maud Land, Antarctica, PhD thesis, University of Bremen, Bremen, Germany, 2014.

Langenfelds, R. L., Guerette E-A., Steele L. P., Krummel P. B., Spencer D. A., Loh Z. M., Gregory R. L., Thornton D. P., Howden R. T. and Fraser P. J.: Atmospheric methane, carbon dioxide, carbon monoxide, hydrogen and nitrous oxide from Cape Grim flask samples analyzed by gas chromatography, in Baseline Atmospheric Program (Australia), 2014-16, R. Langenfelds, N. Derek and S. L. Cleland (eds.), Bureau of Meteorology and CSIRO Environment, Melbourne, Australia, in press, 2023.

Loh, Z., Langenfelds, R., Krummel, P.: Atmospheric CO at Casey by Commonwealth Scientific and Industrial Research Organisation, dataset published as CO_CYA_surface-flask_CSIRO_data1 at WDCGG, ver.2021-04-08-1004, https://doi.org/10.50849/WDCGG_0016-7004-3001-01-02-9999, 2021a.

Loh, Z., Langenfelds, R., Krummel, P.: Atmospheric CO at South Pole by Commonwealth Scientific and Industrial Research Organisation, dataset published as CO_SPO_surface-flask_CSIRO_data1 at WDCGG, ver.2021-04-08-1004, https://doi.org/10.50849/WDCGG_0016-7011-3001-01-02-9999, 2021b.

Loh, Z., Langenfelds, R., Krummel, P.: Atmospheric CO at Mawson by Commonwealth Scientific and Industrial Research Organisation, dataset published as CO_MAA_surface-flask_CSIRO_data1 at WDCGG, ver.2021-04-08-1004, https://doi.org/10.50849/WDCGG_0016-7005-3001-01-02-9999, 2021c.

Masarie, K. A., R. L. Langenfelds, C. E. Allison, T. J. Conway, E. J. Dlugokencky, R. J. Francey, P. C. Novelli, L. P. Steele, P. P. Tans, B. Vaughn and J. W. C. White, NOAA/CSIRO Flask Air Intercomparison Experiment: A strategy for directly assessing consistency among atmospheric measurements made by independent laboratories, J. Geophys. Res., 106, 20445-20464, 2001.

Mitchell, L. E., Brook, E. J., Lee, J. E., Buizert, C. and Sowers, T.: Constraints on the late holocene anthropogenic contribution to the atmospheric methane budget, Science, 342(6161), 964–6, doi:10.1126/science.1238920, 2013.

Morville, J., Kassi, S., Chenevier, M. and Romanini, D.: Fast, low-noise, mode-by-mode, cavity- 7 enhanced absorption spectroscopy by diode-laser self-locking, Appl. Phys. B-Lasers Opt., 80(8), 8 1027–1038, doi:10.1007/s00340-005-1828-z, 2005.

Rhodes, R. H., Faïn, X., Brook, E. J., McConnell, J. R., Maselli, O. J., Sigl, M., Edwards, J. S., Buizert, C., Blunier, T., Chappellaz, J. and Freitag, J.: Local artifacts in ice core methane

records caused by layered bubble trapping and in situ production: a multi-site investigation, Clim. Past, 12(4), 1061–1077, doi:10.5194/cp-12-1061-2016, 2016.

Rommelaere, V., Arnaud, L. and Barnola, J. M.: Reconstructing recent atmospheric trace gas concentrations from polar firn and bubbly ice data by inverse methods, J. Geophys. Res., 102, 30 069-30 083, 1997.

Servettaz, A. P. M., Orsi, A. J., Curran, M. A. J., Moy, A. D., Landais, A., McConnell, J. R., Popp, T. J., Le Meur, E., Faïn, X. and Chappellaz, J.: A 2000-year temperature reconstruction on the East Antarctic plateau from argon–nitrogen and water stable isotopes in the Aurora Basin North ice core, Clim. Past, 19(6), 1125–1152, doi:10.5194/cp-19-1125-2023, 2023.

Trudinger, C. M., Enting, I. G., Rayner, P. J., Etheridge, D. M., Buizert, C., Rubino, M., Krummel, P. B. and Blunier, T.: How well do different tracers constrain the firn diffusivity profile?, Atmos. Chem. Phys., 13(3), 1485–1510, doi:10.5194/acp-13-1485-2013, 2013.

Trudinger, C. M., Fraser, P. J., Etheridge, D. M., Sturges, W. T., Vollmer, M. K., Rigby, M., Martinerie, P., Mühle, J., Worton, D. R., Krummel, P. B., Steele, L. P., Miller, B. R., Laube, J., Mani, F. S., Rayner, P. J., Harth, C. M., Witrant, E., Blunier, T., Schwander, J., O'Doherty, S. and Battle, M.: Atmospheric abundance and global emissions of perfluorocarbons CF_4, C_2F_6 and C_3F_8 since 1800 inferred from ice core, firn, air archive and in situ measurements, Atmos. Chem. Phys., 16(18), 11733–11754, doi:10.5194/acp-16-11733-2016, 2016.

Werle, P., Mücke, R. and Slemr, F.: The Limits of Signal Averaging in Atmospheric Trace-Gas Monitoring by Tunable Diode-Laser Absorption Spectroscopy (TDLAS), Appl. Phys. B-Lasers Opt., 139, 131–139, 1993.

Witrant, E., Martinerie, P., Hogan, C., Laube, J. C., Kawamura, K., Capron, E. and Montzka, S. A., E. J. Dlugokencky,D. Etheridge, T. Blunier, and W. T. Sturges: A new multi-gas constrained model of trace gas non-homogeneous transport in firn : evaluation and behaviour at eleven polar sites, Atmos. Chem. Phys., (12), 11465–11483, doi:10.5194/acp-12-11465-2012, 2012.

Witrant, E. and Martinerie, P.: Input Estimation from Sparse Measurements in LPV Systems and Isotopic Ratios in Polar Firns, IFAC Proc. Vol., 46(2), 659–664, doi:10.3182/20130204-3-FR-2033.00201, 2013.